Graphene-P(VDF-TrFE) Multilayer Film for Flexible Applications

Sang-Hoon Bae,[†,‡] Orhan Kahya,[¶,∥,#] Bhupendra K. Sharma,[‡] Junggou Kwon,[†] Hyoung J. Cho,[§,⊥] Barbaros Özyilmaz,[¶,∥,#,▽,*] and Jong-Hyun Ahn[‡,*]

[†]School of Advanced Materials Science and Engineering and [§]WCU Program, School of Advanced Materials Science and Engineering, Sungkyunkwan University, Suwon 440-746, Korea, [‡]School of Electrical and Electronic Engineering, Yonsei University, Seoul 120-749, Korea, [⊥]Department of Mechanical and Aerospace Engineering, University of Central Florida, Orlando, Florida 32816-2450, United States, [¶]Department of Physics, 2 Science Drive 3, National University of Singapore, Singapore 117542, Singapore, [∥]Graphene Research Centre, 6 Science Drive 2, National University of Singapore, Singapore 117546, Singapore, [#]NanoCore, 4 Engineering Drive 3, National University of Singapore, Singapore 117576, Singapore, and [▽]NUS Graduate School for Integrative Sciences and Engineering (NGS), Centre for Life Sciences (CeLS), 28 Medical Drive, Singapore 117456, Singapore

ABSTRACT A flexible, transparent acoustic actuator and nanogenerator based on graphene/P(VDF-TrFE)/graphene multilayer film is demonstrated. P(VDF-TrFE) is used as an effective doping layer for graphene and contributes significantly to decreasing the sheet resistance of graphene to 188 ohm/sq. The potentiality of graphene/P(VDF-TrFE)/graphene multilayer film is realized in fabricating transparent, flexible acoustic devices and nanogenerators to represent its functionality. The acoustic actuator shows good performance and sensitivity over a broad range of frequency. The output voltage and the current density of the nanogenerator are estimated to be ~3 V and ~0.37 μAcm^{-2}, respectively, upon the application of pressure. These values are comparable to those reported earlier for ZnO- and PZT-based nanogenerators. Finally, the possibility of rollable devices based on graphene/P(VDF-TrFE)/graphene structure is also demonstrated under a dynamic mechanical loading condition.

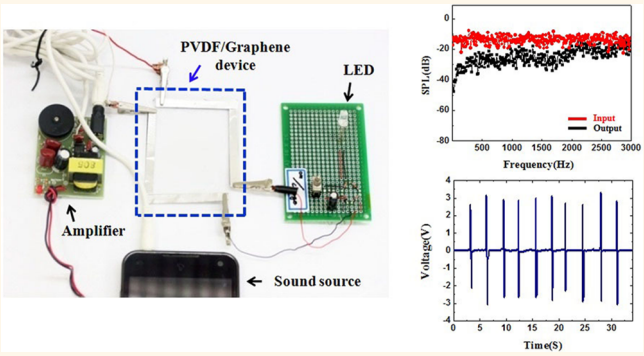

KEYWORDS: CVD graphene · electrostatic doping · actuator · generator · flexible electronics

Currently, indium tin oxide (ITO) thin films with high electrical conductivity and good optical transparency are widely used due to a large demand for transparent electrodes in various electronic applications. An ITO thin film is, however, brittle and often requires an additional annealing step for improvement of its property at high temperature over melting temperature of conventional plastic films. This severely limits its applications to lightweight and flexible devices such as organic solar cells, nonvolatile memory, acoustic actuator, and nanogenerator.[1,2] Graphene, as an alternative to ITO, has recently attracted a great deal of attention owing to its outstanding properties such as high electrical conductivity, good optical transparency, and high mechanical strength.[3−9] To widen the application areas of graphene to various electronic devices and systems, its electrical conductivity must be equivalent to or exceed that of ITO. Moreover, although chemical doping has been generally used, the adsorption of moisture and other chemical molecules under environmental conditions cause serious degradation in electrical conductivity of chemically doped graphene.[10−13] On the other hand, nonvolatile doping by ferroelectric polarization of piezoelectric materials such as $Pb(Zr_xTi_{1-x})O_3$ (PZT) can effectively enhance the conductivity of graphene *via* heavy doping up to 6×10^{12} cm^{-3} and preserve it for a long time with chemical inertness.[14] Although the conductivity of graphene can be significantly improved by utilizing PZT as a substrate, there are significant trade-offs which limit mechanical flexibility and optical transmittance of the completed structure. Recently, as an alternative, the polymer piezoelectric material, poly(vinylidene fluoride-co-trifluoroethylene) (P(VDF-TrFE)), has been exploited as a nonvolatile ferroelectric gating substrate for graphene owing to its good optical transparancy and mechanical flexibility.[15,16]

* Address correspondence to ahnj@yonsei.ac.kr, phyob@nus.edu.sg.

Received for review November 22, 2012 and accepted February 28, 2013.

Published online February 28, 2013
10.1021/nn400848j

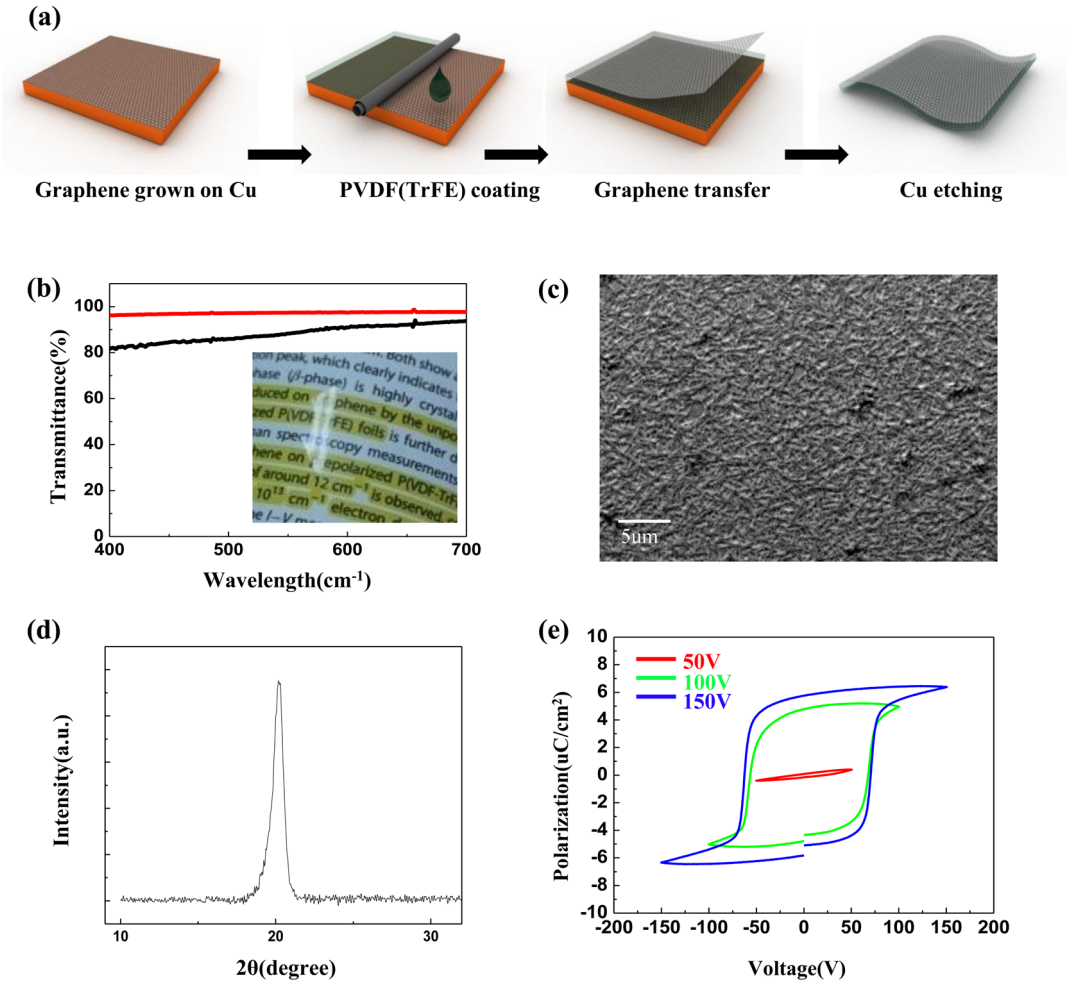

Figure 1. (a) Schematic flow of various key steps during the fabrication of graphene/P(VDF-TrFE)/graphene multilayer film. (b) Transmission spectra of monolayer graphene (97%) and graphene/P(VDF-TrFE) (88%). The inset shows the photograph of transparent graphene/P(VDF-TrFE). (c) SEM image of P(VDF-TrFE) showing its crystallized surface morphology. (d) X-ray diffraction of P(VDF-TrFE) indicating the formation of the beta-phase. (e) Polarization hysteresis loop of the graphene/P(VDF-TrFE)/graphene structure at different applied voltages of 50, 100, and 150 V.

In this paper, we demonstrate applications of P(VDF-TrFE) sandwiched with graphene electrodes to an acoustic actuator and highly efficient nanogenerator. The resulting graphene/P(VDF-TrFE)/graphene multilayer-based actuator and nanogenerator exhibit good mechanical durability and sensitivity, optical transmittance, and simple device design, which is compatible with conventional batch fabrication steps as it is essential for realizing practical devices and systems.

RESULTS AND DISCUSSION

Figure 1a shows the key steps in fabricating the acoustic device of the P(VDF-TrFE) sandwiched between two graphene electrodes. Graphene films were grown on Cu foil using the well-known conventional chemical vapor deposition (CVD) method.[17] P(VDF-TrFE) solution was spin or bar coated on as-grown graphene films and annealed in an oven at 150 °C for 2 h to improve the crystalline nature of coated P(VDF-TrFE) film. A graphene layer was transferred onto the top of the P(VDF-TrFE)/graphene/Cu film and then the Cu foil was etched. Finally, the graphene/P(VDF-TrFE)/graphene sandwiched structure was obtained. To know the effect of coated P(VDF-TrFE) on the transparency of the device, transmittance spectra of bare graphene and P(VDF-TrFE)/graphene was measured as shown in Figure 1b. Figure 1b inset image shows the photograph of the transparent thin graphene/P(VDF-TrFE)/graphene multilayer film. Monolayer graphene shows the ~97% transmission at ~550 nm while it decreases up to ~88% for 30 μm thick P(VDF-TrFE)/graphene films.[18,19] The surface morphology and crystalline quality of P(VDF-TrFE) film were investigated by scanning electron micrscopy (SEM), X-ray diffraction (XRD), and Fourier transform infrared spectroscopy (FTIR). A SEM image of P(VDF-TrFE) film exhibits the formation of needle-like crystals and uniform growth (Figure 1c).[20] The XRD of P(VDF-TrFE) exhibits a single peak at 20° as shown in Figure 1d, indicating the formation of the beta phase, which exhibits good piezoelectric properties. In addition, FTIR measurement shows only two

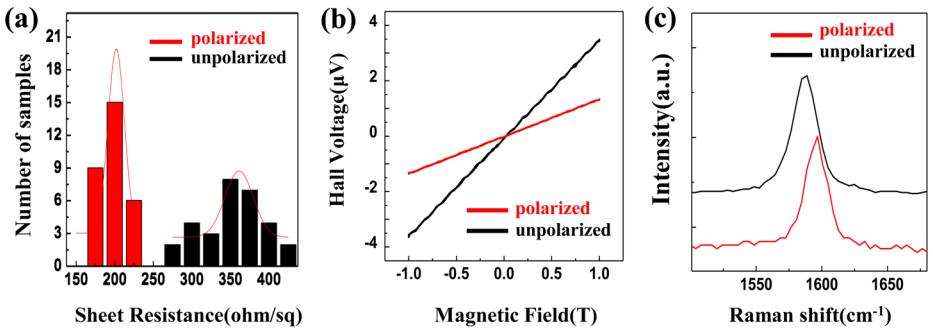

Figure 2. (a) Measurement of sheet resistance of graphene on P(VDF-TrFE) with and without polarization. Gaussian distribution shows the average value indicating the lower sheet resistance for polarized specimen. (b) Variation of Hall voltage with respect to applied magnetic field with and without poling. (c) Raman spectrum shows the red shift in the G peak position for the polarized sample as compared to the unpolarized one.

specific peaks (600 and 840 cm^{-1}) of the beta phase without other peaks related to other phases (Supporting Information, Figure S1).[21−23] Therefore, the formation of only the beta phase in as-synthesized P(VDF-TrFE) will allow us to use it in fabricating the electromechanical devices. Further, the piezoelectric properties of P(VDF-TrFE) film with a thickness of 1 μm were confirmed by measuring the hysteresis loop ($P-V$ curve) with respect to different voltage sweeping ranges. $P-V$ curves were measured in the ranges of ±50, 100, and 150 V, which result in the corresponding polarization values of 0.5, 5.2, and 6.4 $\mu C/cm^2$, respectively (Figure 1e). The calculated dielectric constants at 50 V, 100 V, and 150 V are ∼11.3, 58.7, and 48.2, respectively, which are comparable to those observed in high quality P(VDF-TrFE).[16,24,25] The root-mean-square (RMS) value on the surface of the P(VDF-TrFE) film was estimated as ∼22 nm as revealed by the atomic force microscopy image (Supporting Information, Figure S2).

It is noteworthy to investigate the effect of solution casting ferroelectric P(VDF-TrFE) polymer film over graphene as dipoles of ferroelectric polymer significantly affect the amount of charge carriers in graphene, as poling causes the polarization of P(VDF-TrFE).[24] The electrical properties of graphene film sandwiching P(VDF-TrFE)s before and after the poling process were evaluated in terms of sheet resistance and carrier concentration measured in a standard van der Pauw geometry. Figure 2a shows the measurement of sheet resistance for two kinds of specimens (before and after poling) and the average sheet resistance of 30 samples from each kind are represented with Gaussian fitting. The mean value of the sheet resistance of graphene films on P(VDF-TrFE) with poling was found to be ∼188 ohm/sq, while that of the sample without poling showed ∼353 ohm/sq. The decrease of sheet resistance in graphene over polarized P(VDF-TrFE) polymer indicates doping effects induced by polarization of the polymer. Here, the doping phenomenon caused by the polarization of P(VDF-TrFE) between two graphene films can be understood qualitatively. One can expect the p-type doping could take place if charge transfer occurs at the interface between graphene and P(VDF-TrFE) fluoropolymer. Charge transfer phenomenon between two dissimilar materials significantly depends on the difference of their Fermi levels. However, P(VDF-TrFE) is an insulating polymer and it has lower electron affinity as compared to graphene work function. Therefore, in the present case the possibility of charge transfer phenomenon between graphene and P(VDF-TrFE) does not seem to be reasonable for doping in graphene. Alternatively, doping behavior in graphene can be understood in terms of electrostatic potential created by the dipoles in P(VDF-TrFE) fluoropolymer as described in an earlier report to understand the doping by self-assembled monolayers (SAMs) on monolayer graphene.[26,27] In our case, synthesized P(VDF-TrFE) exhibits a beta phase in which dipole moments of C−F and C−H bonds add up contributing an effective dipole moment in a direction perpendicular to carbon backbone especially after the poling process. These effective dipole moments on the graphene basal plane significantly shift the Fermi level downward resulting in the doping in graphene. It is well-known that the CVD grown graphene can have a large number of specific charged impurities, such as nonuniform p-type doping due to etching and transferring process. Therefore, the formation of two kinds of junctions at the graphene/P(VDF-TrFE) interface could be possible depending on the nature of remnant polarization. When P(VDF-TrFE) is subjected to the negative remnant polarization, the dipoles at the graphene/P(VDF-TrFE) interface form the p−p junction and decrease the overall sheet resistance of graphene with hole doping. On the other hand, when P(VDF-TrFE) is subjected to the positive remnant polarization, then dipoles at the graphene/P(VDF-TrFE) interface can form the p−n junction and increase the overall sheet resistance of graphene with electrostatic n-type doping. The formation of p−n junction provides the potential step for the current path and thus increases the sheet resistance, whereas the formation of p−p junction provides a smooth current path way and decreases the sheet

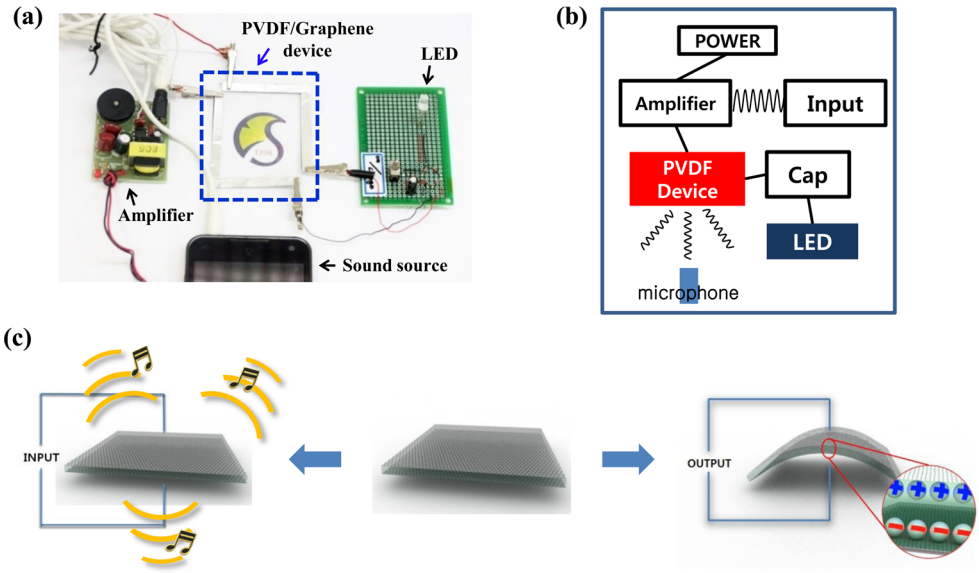

Figure 3. (a) Photograph showing the electrical connections of sound source, amplifier, graphene/P(VDF-TrFE)/graphene-based acoustic device and electrical circuit with red LED during the measurement. (b) Schematic representation of electrical circuit including the entire component in the measurement of acoustic device. (c) Schematic depiction showing graphene/P(VDF-TrFE)/graphene-based device can work as an actuator as well as a nanogenerator.

resistance.[16] Since doping in graphene can lead to an increment of carrier concentration, the carrier concentration for both kinds of specimens using unpolarized P(VDF-TrFE) and polarized P(VDF-TrFE) was calculated through a Hall-effect measurement. Figure 2b shows the variation of Hall-voltage with respect to applied magnetic field. The slope of polarized P(VDF-TrFE) specimen decreases as compared to unpolarized P(VDF-TrFE). The numerical value of carrier concentration can be calculated by the following expression:

$$n = \frac{1}{e \times \text{slope}} \quad \text{slope} = \frac{V_h}{B}$$

Where n and e represent the carrier concentration and the electronic charge, respectively. Slopes for unpolarized P(VDF-TrFE) and polarized P(VDF-TrFE) are estimated as 3.46×10^{-6} V/T and 1.31×10^{-6} V/T and their corresponding carrier concentration are found to be $\sim 6.8 \times 10^{12}$ cm^{-3} and $\sim 1.8 \times 10^{13}$ cm^{-3}, respectively. The increment of carrier concentration for the poled P(VDF-TrFE) as compared to one without poling indicates the significant electrostatic doping due to P(VDF-TrFE). The doping effect was also observed in Raman study. Figure 2c shows the relative change in "G" peak position of graphene film over unpolarized P(VDF-TrFE) and polarized P(VDF-TrFE). The position of the G peak is observed at 1586.8 cm^{-1} without polarization and at 1594 cm^{-1} with polarization. It is well-known that the position of G peak changes depending on the doping effect. It has been reported that the doping in graphene causes the phonon stiffening effect by charge extraction resulting in the upshift in the G peak. Therefore, the observed shift in G peak position again gives the indication of doping which matches with the earlier reported work.[28] The above-described results, including Hall effect measurement and Raman shift, and discussion conclude that the P(VDF-TrFE) fluoropolymer can be used to increase the conductivity of graphene by significant p-type doping to make it comparable to ITO. Additionally it is also important that there is no other supporting substrate required to handle the graphene/P(VDF-TrFE)/graphene structure, which is needed for the fabrication of electromechanical devices.

To show the potential of the graphene/P(VDF-TrFE) multilayer structure for electromechanical devices, we fabricated the graphene/P(VDF-TrFE)/graphene-based acoustic actuator and nanogenerator. Figure 3a illustrates the complete picture of electronic circuitry during the measurement of graphene/P(VDF-TrFE)/graphene-based acoustic actuator and nanogenerator. A schematic representation of electronic circuit is shown in Figure 3b. To characterize the performance of graphene/P(VDF-TrFE)/graphene-based transducer, the device was excited to produce sound in which an amplified electrical driving signal was used within a broad frequency range using the white noise signal.[29] An amplified signal was propagated to the fabricated acoustic device based on the graphene/P(VDF-TrFE)/graphene structure. The graphene/P(VDF-TrFE)/graphene device produces acoustical pressure or mechanical vibrations in response to the input electrical signal. These mechanical vibrations were sensed by the microphone. The distance between the microphone and the fabricated acoustic device was kept to ~50 mm. This test was performed in an anechoic room to avoid any external noise. The anechoic room was designed to act

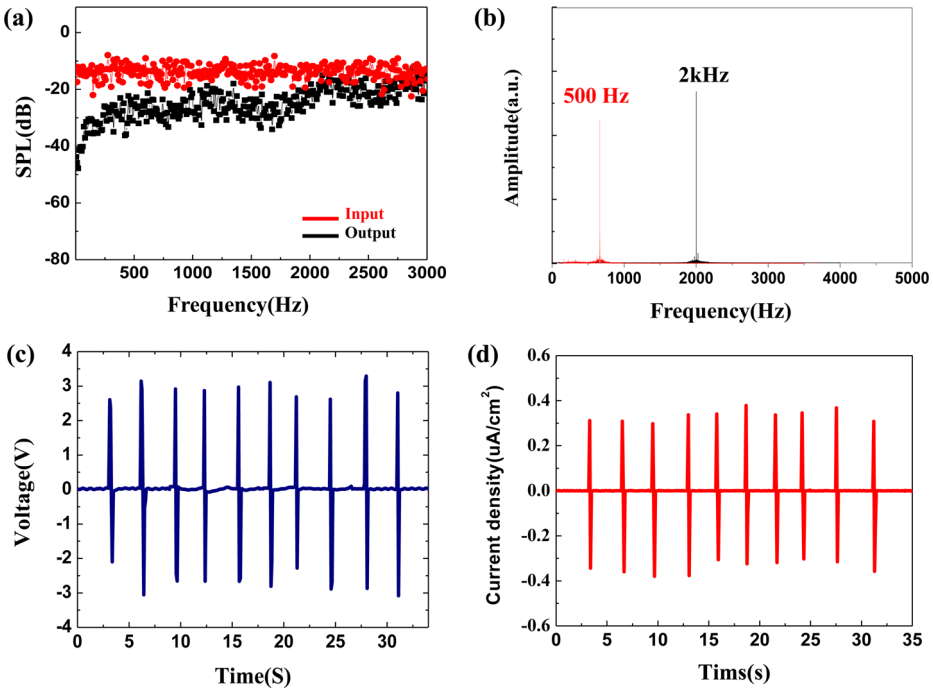

Figure 4. (a) Frequency response in the test using white noise signal: variation of sound pressure level (SPL) with respect to frequency within the broad region (1−3000 Hz). (b) Output response of graphene/P(VDF-TrFE)/graphene-based acoustic device at particular frequencies. (c) Output voltage and (d) current density of graphene/P(VDF-TrFE)/graphene based nanogenerator with respect to time.

as block reflector for sound signals and electromagnic waves, and was kept isolated from an external source of noise, providing an open space of infinite dimension.[30] In addition, this device could generate output voltage which was used to turn on a LED by continuosly bending/unbending the graphene/P(VDF-TrFE)/graphene-based device. That is, continuos bending/unbending converted the mechanical energy applied on graphene/P(VDF-TrFE)/graphene device to electrical energy which was able to drive the LED. In this way the fabricated graphene/P(VDF-TrFE)/graphene-based acoustic device can be utilized to sense the electrical signal by producing the mechanical vibration and also to drive the LED by converting the mechanical energy to electrical energy as shown in Figure 3c. The energy conversion and the actuation behavior of graphene/(PVDF-TrFE)/graphene structure is due to the piezoelectric property of PVDF-TrFE. When PVDF-TrFE thin film sandwiched between two graphene electrodes is subjected to external mechanical stress (in case of nanogenerator), dipoles inside the PVDF-TrFE thin film start to align in perpendicular direction to the plane of thin film. Therefore, significant opposite charges can accumulate on the top and bottom surfaces of the PVDF-TrFE film, which can further be extracted out through the external electronic circuitry. The actuation of the graphene/(PVDF-TrFE)/graphene structure is created by this process in reverse. In addition to acoustic actuators by use of piezoelectric materials, considerable research has recently been undertaken on graphene-based electrochemical and bimorph-type actuators.[31−34]

The as-fabricated graphene/P(VDF-TrFE)/graphene-based device was tested under several conditions to investigate its performance as the acoustic actuator and the nanogenerator. Figure 4a shows a frequency response of the fabricated acoustic device within the frequency range of 1−3000 Hz. Here, we followed C-weighted measurement using the white noise signal. The speaker showed a smooth response over a broad range of frequency region. The output was converted in to sound pressure level (SPL) with the help of fast Fourier transformation (FFT) using the following expression:

$$\mathrm{SPL} = 10 \log \frac{I_x}{I_r} = 20 \log \frac{P_x}{P_r}, \quad I = \frac{P^2}{\rho v}$$

Here, I, ρv, P_x, and P_r represent a sound intensity, an acoustic impedance, an effective value of measured pressure, and a reference value of effective pressure, respectively. A reference value of pressure (P_r) of ~20 μPa was used for the calculation. In the present study, the fabricated graphene/P(VDF-TrFE)/graphene-based acoustic device showed a little inconsistency in response to the input signal (Figure 4a), but it is far better than that of earlier reported CNT[29]-based transparent acoustic actuator in tests using white noise signal. In addition, compared to reduced graphene oxide (RGO),[35] CVD-grown graphene has an advantage in terms of low power consumption due to superior electrical conductivity. During this test, the device performance was measured in response to a broad

frequency range, so we could not check the ability to obtain a response at a particular frequency without any distortion. Therefore, to check the device sensitivity at a particular frequency, the signals of 500 Hz frequency and 2 kHz frequency, which lie in the bass and middle frequency range, respectively, were applied for 5 s. A similar calculation was done by using the FFT to obtain the output result, which is shown in Figure 4b. The sharp resonance peak with full width half-maximum FWHM < 0.4 Hz and weak shoulder were observed as an output at 500 Hz and 2 kHz frequency, respectively, which indicates a good sensitivity of the graphene/P(VDF-TrFE)/graphene-based acoustic actuator. The above result shows the potential of the graphene/P(VDF-TrFE)/graphene-based acoustic device which can operate very well within the broad frequency range. The use of a graphene electrode in the present fabricated device fulfills the requirement of mechanical endurance and good conductivity as well as high transparency, which makes it superior over other ITO, conductive polymer, and CNTs-based acoustic devices. Its high transparency, good flexibility, and deletion of the requirement for a supporting substrate make it appropriate to easily integrate in any transparent flexible system such as touch screens, smart windows, and e-papers to name a few among many future applications. In addition, it employs a low processing cost with low cost materials which will provide an easy pathway to commercialization of such devices based on the graphene/P(VDF-TrFE)/graphene structure. In addition, the sound propagation phenomenon of thin film-based speakers is quite different from traditional speakers, which is advantageous. In the case of a thin film speaker, the sound propagates from everywhere over a large size panel, whereas in traditional speakers the sound comes only from one point where the actuator is actually installed. The ability of thin film speakers to produce the sound from over all the surface provides a better stereo height and width making it superior to traditionally available speakers.

Exploiting the piezoelectric property of a P(VDF-TrFE) fluoropolymer, the graphene/P(VDF-TrFE)/graphene-based nanogenerator has been demonstrated, and successfully used to turn on a red LED (Supporting Information, Figure S3) which can be lighted up over 1.7 V. The forward-biased resistance is 450 ohm and an emission spectrum is centered at 635 nm. To characterize the performance of the nanogenerator, a nanovoltmeter and a picoammeter were used to detect generated voltage and current density, respectively, with respect to time, and a labview program was used to monitor the output signals. Strain was applied to the graphene/P(VDF-TrFE)/graphene film in a cyclic manner with compression and release stages using the bending machine. During the bending test, the applied strain value was ~0.3% and the strain rate was 60 mm/s. Figure 4c and d show the variation of output voltage and current density as a function of time of fabricated nanogenerator. The graphene/P(VDF-TrFE)/graphene-based nanogenerator showed stable performance, and the average output voltage was observed as ~2.5 V, while its maximum value was found to be ~3 V. The average output of current density was found to be over ~0.2 μAcm^{-2}, while the maximum value was estimated to be ~0.37 μAcm^{-2}. In addition, the long-term-stability test for nanogenerator operation was carried out for 10 min (cycling of >500 times) (Supporting Information, Figure S4). The result indicates good stability of output magnitude. The energy conversion efficiency of the device, which is defined as the ratios between the energies corresponding to applied strain (input) and the electrical response (output), is 8%.[36] (Supporting Information). Although a high performance of nanogenerators could be recently achieved by using low temperature and cost-effective processes,[37−40] the output voltage and functionality of graphene/P(VDF-TrFE)/graphene-based nanogenerators are comparable to those of common ZnO- and PZT-based ones.[41−43]

The obtained output voltage of ~2 V can be more than sufficient to turn on the LED. A red LED was connected to the output of a graphene/P(VDF-TrFE)/graphene nanogenerator using the well-known charging-discharging electrical circuit in two steps (inset of Supporting Information, Figure S3). In the first step, the output voltage of the nanogenerator was rectified using four diodes, and then the capacitor was charged by connecting the switch "A". In the second step, the charge capacitor was used to turn on the LED by connecting the switch "B". Supporting Information, Figure S3 demonstrates the successful illumination of the red LED using the voltage generated from the fabricated nanogenerator in response to the external mechanical force. To get a good performance out of the nanogenerator, the top and bottom electrodes play a crucial role, as these are responsible for charge collection at the interfaces. In the present work, it is expected that the nonvolatile doping of the ferroelectric P(VDF-TrFE) polymer in graphene significantly decreases the sheet resistance and lowers the barrier in collecting the charges from the P(VDF-TrFE) to the graphene electrode at the interface, resulting in the excellent performance of the nanogenerator. The other important advantage of the fabricated nanogenerator in the present work is its easy fabrication, which makes it quite different from previously reported ones and indicates that the graphene/P(VDF-TrFE)/graphene-based structures can be utilized as an acoustic actuator as well as a nanogenerator representing its functionality.

Moreover, because of the increasing demand of rollable devices in the next generation of flexible electronics, rollability testing of the graphene/P(VDF-TrFE) structure was performed. Figure 5a shows the graphene/P(VDF-TrFE) structure mounted on a rollable machine in which one edge of the sample was

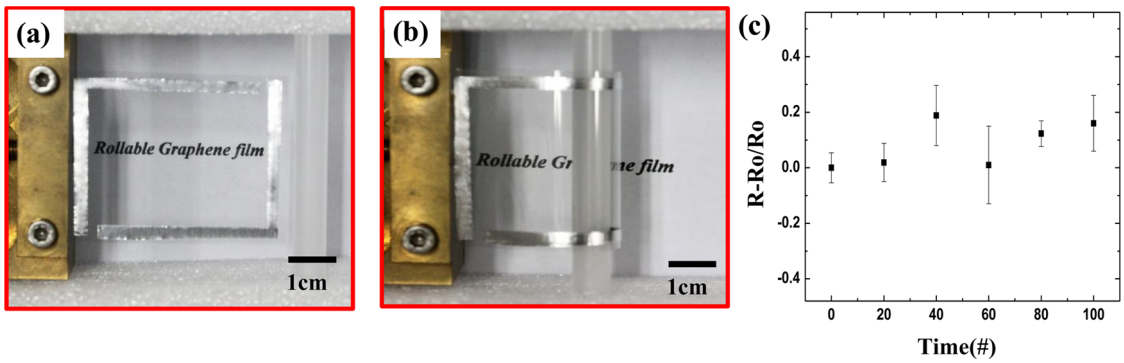

Figure 5. (a) Demonstration of rollability of graphene/P(VDF-TrFE)/graphene multilayer structure. Photograph of graphene/P(VDF-TrFE)/graphene film (a) before and (b) after rolling. (c) Variation of normalized sheet resistance with respect to number of rolling cycles.

fastened at the flat tip of the machine and other edge of the sample was fixed at the opposite roller. Figure 5b shows a mounted structure in the rolling mode. The structure was rolled and released up to 100 cycles, and the resistance of the graphene film was measured. Figure 5c shows the variation of resistance as a function of a number of cycles. The relative change of resistance of graphene/P(VDF-TrFE) film was found to be within the range of 0.2. The graphene/P(VDF-TrFE) film shows the consistent performance under the rolling test and demonstrates the possibility of fabricating the rollable acoustic actuator and nanogenerator devices. The strain value experienced by the graphene/P(VDF-TrFE) structure during the rolling test can be estimated using the following equation;[44]

$$\epsilon = \left(\frac{d_s + d_f}{2R}\right)\frac{(1 + 2\eta + \chi\eta^2)}{(1 + \chi\eta)(1 + \eta)}, \quad \eta = d_s/d_f \quad \text{and} \quad \chi = Y_s/Y_f$$

Here, d_s and d_f represent the thickness of surface and substrate film while Y_s and Y_f represent its Young's modulus, respectively. R is the radius of employed roller during the rolling test, which is ~7 mm. In the present case, d_s is used as ~0.3 nm and d_f as ~30 μm. Young's modulus of graphene and PVDF(TrFE) can be used as ~1 Tpa and ~1 GPa.[45,46] By inserting the numerical values of all the parameters in the above equation, the applied value of strain in the graphene is estimated to be ~0.21%, where graphene resistance did not change abruptly. Here, for the strain calculation, we used the Young's modulus value of exfoliated graphene. However it does not much affect our calculation as the main contribution to the strain value significantly depends on the thickness of the total device and cylinder radius rather than the value of Young's modulus.

CONCLUSION

In summary, an acoustic actuator and a nanogenerator were fabricated based on a graphene/P(VDF-TrFE)/graphene film. A stand-alone P(VDF-TrFE)/graphene structure could be realized at low processing temperature without using any supporting substrate such as PET for extra fabrication steps. The fluoropolymer P(VDF-TrFE) when laminated with graphene significantly increased the conductivity of graphene films by a p-type doping effect due to dipole moment interactions at the interface. The type of doping was experimentally confirmed by Hall measurement, and the doping signature was also observed in Raman spectrum. The frequency response of the acoustic actuator showed consistent operation and was recorded with a sharp resonance peak, which indicates a good sensitivity. The performance charateristics such as output voltage and current density exceeded those values reported in the ZnO- and PZT-based nanogenerators. Finally, the potential of rollable devices was explored using a graphene/P(VDF-TrFE)/graphene-based film. Our work demonstrated the applications of graphene/organic films, presenting a viable approach to developing integrated acoustic devices and self-powered systems.

EXPERIMENTAL METHODS

Multilayer Film Fabrication. A monolayer graphene was prepared on a Cu foil (25 μm) using the CVD method. First, Cu foil was loaded in the thermal CVD and the temperature was increased up to 1000 °C with flowing 8 sccm of H_2 at 90 mtorr. At 1000 °C, the sample was annealed for 30 min with flowing 20 sccm of CH_4, and then it was cooled to room temperature with flowing 8 sccm of H_2. Subsequently, the P(VDF-TrFE), which dissolved in a dimethylformamide (DMF) solvent, was coated directly on top of the graphene. The back-side of the graphene was etched by a reactive ion etcher at 100 W for 4 s. To make crystallized P(VDF-TrFE), it was annealed at 150 °C for 2 h. The graphene was transferred to the top of P(VDF-TrFE) film again, and the Cu foil was etched using an aqueous ammonium persulfate solution. Finally, the graphene/P(VDF-TrFE)/graphene film was formed.

Device Characterization. The graphene/P(VDF-TrFE)/graphene film is excited to produce sound by driving signals, such as

white noise signal and 500 Hz or 2 kHz frequency, to characterize the performance of an acoustic actuator. An amplified signal was propagated, which caused mechanical vibrations or acoustical pressure. To sense vibrations, a microphone was used at 50 mm distance from the device in the anechoic room, which was designed to block external signals. To measure the performance of the generator, the multilayer film was installed on the bending machine with a step motor and then the strain of ~0.3% with the strain rate of 60 mm/s was applied to produce electrical signal. The output voltage and output current density were measured by nanovoltmeter (Kithley 2182A) and a picoammeter (Kithley 6485), respectively.

Conflict of Interest: The authors declare no competing financial interest.

Acknowledgment. This work was supported by the Basic Research Program (2012R1A2A1A03006049 and 2009-0083540) and Global Frontier Research Center for Advanced Soft Electronics (2011-0031635) through the National Research Foundation of Korea (NRF), funded by the Ministry of Education, Science and Technology and the Technology Innovation Program (Grant 10041066) funded by the Ministry of Knowledge Economy (MKE), Korea; the Singapore National Research Foundation Grants NRF-RF2008-07 and NRF-CRP "Toward Commercialization of Graphene Technologies" (R-144-000-315-281); NUS-YIA award (R144-000-283-101); A*STAR SERC TSRP-Integrated Nanophoto-Bio Interface (R-144-000-275-305); and U.S. Office of Naval Research (ONR and ONR Global).

Supporting Information Available: IR spectra of the P(VDF-TrFE) crystallized from annealing at 150 °C (Figure S1); atomic force microscopy image of crystallized P(VDF-TrFE) showing its topography (Figure S2); demonstration of successful driving of red LED by applying the output voltage generated from graphene/P(VDF-TrFE)/graphene-based nanogenerator when it is subjected to bending cycles. Inset shows the electrical circuit for driving the LED (Figure S3); result of the stability test from P(VDF-TrFE) device (Figure S4); energy conversion efficiency. This material is available free of charge *via* the Internet at http://pubs.acs.org.

REFERENCES AND NOTES

1. Kim, K. S.; Zhao, Y.; Jang, H.; Lee, S. Y.; Kim, J. M.; Kim, K. S.; Ahn, J.-H.; Kim, P.; Choi, J.-Y.; Hong, B. H. Large-Scale Pattern Growth of Graphene Films for Stretchable Transparent Electrodes. *Nature* **2009**, *457*, 706–710.
2. Kumar, A.; Zhou, C. The Race To Replace Tin-Doped Indium Oxide: Which Material Will Win? *ACS Nano* **2010**, *4*, 11–14.
3. Lee, S.-K.; Kim, B. J.; Jang, H.; Yoon, S. C.; Lee, C.; Hong, B. H.; Rogers, J. A.; Cho, J. H.; Ahn, J.-H. Stretchable Graphene Transistors with Printed Dielectrics and Gate Electrodes. *Nano Lett.* **2011**, *11*, 4642–4646.
4. Liu, Z.; Liu, Q.; Huang, Y.; Ma, Y.; Yin, S.; Zhang, X.; Sun, W.; Chen, Y. Organic Photovoltaic Devices Based on a Novel Acceptor Material: Graphene. *Adv. Mater.* **2008**, *20*, 3924–3930.
5. Han, T.-H.; Lee, Y.; Choi, M.-R.; Woo, S.-H.; Bae, S.-H.; Hong, B. H.; Ahn, J.-H.; Lee, T.-W. Extremely Efficient Flexible Organic Light-Emitting Diodes with Modified Graphene Anode. *Nat. Photon.* **2012**, *6*, 105–110.
6. Kim, R.-H.; Bae, M.-H.; Kim, D. G.; Cheng, H.; Kim, B. H.; Kim, D.-H.; Li, M.; Wu, J.; Du, F.; Kim, H.-S.; *et al*. Stretchable, Transparent Graphene Interconnects for Arrays of Microscale Inorganic Light Emitting Diodes on Rubber Substrates. *Nano Lett.* **2011**, *11*, 3881–3886.
7. Rogers, J. A. Electronic Materials: Making Graphene for Macroelectronics. *Nat. Nanotechnol.* **2008**, *3*, 254–255.
8. Bonaccorso, F.; Sun, Z.; Hasan, T.; Ferrari, A. C. Graphene Photonics and Optoelectronics. *Nat. Photon.* **2010**, *4*, 611–622.
9. Bae, S.-H.; Lee, Y.; Sharma, B. K.; Lee, H.-J.; Kim, J.-H.; Ahn, J.-H. Graphene-Based Transparent Strain Sensor. *Carbon* **2013**, *51*, 236–242.
10. Chandra, B.; Afzali, A.; Khare, N.; El-Ashry, M. M.; Tulevski, G. S. Stable Charge-Transfer Doping of Transparent Single-Walled Carbon Nanotube Films. *Chem. Mater.* **2010**, *22*, 5179–5183.
11. Dong-Wook, S.; Jong Hak, L.; Yu-Hee, K.; Seong Man, Y.; Seong-Yong, P.; Ji-Beom, Y. A Role of HNO_3 on Transparent Conducting Film with Single-Walled Carbon Nanotubes. *Nanotechnology* **2009**, *20*, 475703.
12. Yan, C.; Kim, K.-S.; Lee, S.-K.; Bae, S.-H.; Hong, B. H.; Kim, J.-H.; Lee, H.-J.; Ahn, J.-H. Mechanical and Environmental Stability of Polymer Thin-Film-Coated Graphene. *ACS Nano* **2011**, *6*, 2096–2103.
13. Hellstrom, S. L.; Vosgueritchian, M.; Stoltenberg, R. M.; Irfan, I.; Hammock, M.; Wang, Y. B.; Jia, C.; Guo, X.; Gao, Y.; Bao, Z. Strong and Stable Doping of Carbon Nanotubes and Graphene by MoOx for Transparent Electrodes. *Nano Lett.* **2012**, *12*, 3574–3580.
14. Yi, Z.; Guang-Xin, N.; Sukang, B.; Chun-Xiao, C.; Orhan, K.; Chee-Tat, T.; Hye, Ri, K.; Danho, I.; Ting, Y.; Jong Hyun, A.; *et al*. Wafer-Scale Graphene/Ferroelectric Hybrid Devices for Low-Voltage Electronics. *Europhys. Lett.* **2011**, *93*, 17002.
15. Zheng, Y.; Ni, G.-X.; Toh, C.-T.; Tan, C.-Y.; Yao, K.; Özyilmaz, B. Graphene Field-Effect Transistors with Ferroelectric Gating. *Phys. Rev. Lett.* **2010**, *105*, 166602.
16. Ni, G.-X.; Zheng, Y.; Bae, S.; Tan, C. Y.; Kahya, O.; Wu, J.; Hong, B. H.; Yao, K.; Özyilmaz, B. Graphene−Ferroelectric Hybrid Structure for Flexible Transparent Electrodes. *ACS Nano* **2012**, *6*, 3935–3942.
17. Li, X.; Cai, W.; An, J.; Kim, S.; Nah, J.; Yang, D.; Piner, R.; Velamakanni, A.; Jung, I.; Tutuc, E.; *et al*. Large-Area Synthesis of High-Quality and Uniform Graphene Films on Copper Foils. *Science* **2009**, *324*, 1312–1314.
18. Bae, S.; Kim, H.; Lee, Y.; Xu, X.; Park, J.-S.; Zheng, Y.; Balakrishnan, J.; Lei, T.; Ri Kim, H.; Song, Y. I.; *et al*. Roll-To-Roll Production of 30-Inch Graphene Films for Transparent Electrodes. *Nat. Nanotechnol.* **2010**, *5*, 574–578.
19. Nair, R. R.; Blake, P.; Grigorenko, A. N.; Novoselov, K. S.; Booth, T. J.; Stauber, T.; Peres, N. M. R.; Geim, A. K. Fine Structure Constant Defines Visual Transparency of Graphene. *Science* **2008**, *320*, 1308.
20. Park, Y. J.; Kang, S. J.; Park, C.; Woo, E.; Shin, K.; Kim, K. J. Recovery of Remanent Polarization of Poly(vinylidene fluoride-co-trifluoroethylene) Thin Film after High Temperature Annealing Using Topographically Nanostructured Aluminium Bottom Electrode. *Appl. Phys. Lett.* **2007**, *90*, 222903–3.
21. Kusuma, D. Y.; Nguyen, C. A.; Lee, P. S. Enhanced Ferroelectric Switching Characteristics of P(VDF-TrFE) for Organic Memory Devices. *J. Phys. Chem. B* **2010**, *114*, 13289–13293.
22. Gregorio, R., Jr.; Ueno, E. M. Effect of Crystalline Phase, Orientation and Temperature on the Dielectric Properties of Poly(vinylidene fluoride) (PVDF). *J. Mater. Sci.* **1999**, *34*, 4489–4500.
23. Simoes, R.; Rodriguez-Perez, M.; de Saja, J.; Constantino, C. Thermomechanical Characterization of PVDF and P(VDF-TrFE) Blends Containing Corn Starch and Natural Rubber. *J. Therm. Anal. Calorim.* **2010**, *99*, 621–629.
24. Sencadas, V.; Lanceros-Méndez, S.; Mano, J. F. Characterization of Poled and Non-Poled β-PVDF Films Using Thermal Analysis Techniques. *Thermochim. Acta* **2004**, *424*, 201–207.
25. Guo, S. S.; Lau, S. T.; Chan, H. L. W.; Zhao, X. Z.; Choy, C. L. Structural Evolution and Dielectric Relaxation Behavior of Electron-Irradiated Poly(vinylidene fluoride-trifluoroethylene) 80/20 mol% Copolymers. *J. Appl. Phys.* **2003**, *94*, 5566–5573.
26. Yokota, K.; Takai, K.; Enoki, T. Carrier Control of Graphene Driven by the Proximity Effect of Functionalized Self-assembled Monolayers. *Nano Lett.* **2011**, *11*, 3669–3675.
27. Wang, R.; Wang, S.; Zhang, D.; Li, Z.; Fang, Y.; Qiu, X. Control of Carrier Type and Density in Exfoliated Graphene by Interface Engineering. *ACS Nano* **2010**, *5*, 408–412.
28. Rao, A. M.; Eklund, P. C.; Bandow, S.; Thess, A.; Smalley, R. E. Evidence for Charge Transfer in Doped Carbon Nanotube Bundles from Raman Scattering. *Nature* **1997**, *388*, 257–259.

29. Yu, X.; Rajamani, R.; Stelson, K. A.; Cui, T. Carbon Nanotube-Based Transparent Thin Film Acoustic Actuators and Sensors. *Sensors Actuat. A: Phys.* **2006**, *132*, 626–631.
30. Benson, R. W.; Huntley, R., The Effect of Room Characteristics on Sound Power Measurements. *Noise Control* **1959**, *5*, 59-63, 77.
31. Zhu, S.-E.; Shabani, R.; Rho, J.; Kim, Y.; Hong, B. H.; Ahn, J.-H.; Cho, H. J. Graphene-Based Bimorph Microactuators. *Nano Lett.* **2011**, *11*, 977–981.
32. Huang, Y.; Liang, J.; Chen, Y. The Application of Graphene Based Materials for Actuators. *J. Mater. Chem.* **2012**, *22*, 3671–3679.
33. Liang, J.; Huang, L.; Li, N.; Huang, Y.; Wu, Y.; Fang, S.; Oh, J.; Kozlov, M.; Ma, Y.; Li, F.; *et al*. Electromechanical Actuator with Controllable Motion, Fast Response Rate, and High-Frequency Resonance Based on Graphene and Polydiacetylene. *ACS Nano* **2012**, *6*, 4508–4519.
34. Liang, J.; Xu, Y.; Huang, Y.; Zhang, L.; Wang, Y.; Ma, Y.; Li, F.; Guo, T.; Chen, Y. Infrared-Triggered Actuators from Graphene-Based Nanocomposites. *J. Phys. Chem. C* **2009**, *113*, 9921–9927.
35. Shin, K.-Y.; Hong, J.-Y.; Jang, J. Flexible and Transparent Graphene Films as Acoustic Actuator Electrodes Using Inkjet Printing. *Chem. Commun.* **2011**, *47*, 8527–8529.
36. Lee, J.-H.; Lee, K. Y.; Kumar, B.; Tien, N. T.; Lee, N.-E.; Kim, S.-W. Highly Sensitive Stretchable Transparent Piezoelectric Nanogenerators. *Energy Environ. Sci.* **2013**, *6*, 169–175.
37. Zhu, G.; Wang, A. C.; Liu, Y.; Zhou, Y.; Wang, Z. L. Functional Electrical Stimulation by Nanogenerator with 58 V Output Voltage. *Nano Lett.* **2012**, *12*, 3086–3090.
38. Yang, Y.; Guo, W.; Pradel, K. C.; Zhu, G.; Zhou, Y.; Zhang, Y.; Hu, Y.; Lin, L.; Wang, Z. L. Pyroelectric Nanogenerators for Harvesting Thermoelectric Energy. *Nano Lett.* **2012**, *12*, 2833–2838.
39. Hu, Y.; Lin, L.; Zhang, Y.; Wang, Z. L. Replacing a Battery by a Nanogenerator with 20 V Output. *Adv. Mater.* **2012**, *24*, 110–114.
40. Lee, S.; Hong, J.-I.; Xu, C.; Lee, M.; Kim, D.; Lin, L.; Hwang, W.; Wang, Z. L. Toward Robust Nanogenerators Using Aluminum Substrate. *Adv. Mater.* **2012**, *24*, 4398–4402.
41. Kwon, J.; Seung, W.; Sharma, B. K.; Kim, S.-W.; Ahn, J.-H.; High, A. Performance PZT Ribbon-Based Nanogenerator Using Graphene Transparent Electrodes. *Energ. Environ. Sci.* **2012**, *5*, 8970–8975.
42. Lee, M.; Bae, J.; Lee, J.; Lee, C.-S.; Hong, S.; Wang, Z. L. Self-Powered Environmental Sensor System Driven by Nanogenerators. *Energ. Environ. Sci.* **2011**, *4*, 3359–3363.
43. Kumar, B.; Kim, S.-W. Energy Harvesting Based on Semiconducting Piezoelectric ZnO Nanostructures. *Nano Energy* **2012**, *1*, 342–355.
44. Suo, Z.; Ma, E. Y.; Gleskova, H.; Wagner, S. Mechanics of Rollable and Foldable Film-on-Foil Electronics. *App. Phys. Lett.* **1999**, *74*, 1177–1179.
45. Lee, C.; Wei, X.; Kysar, J. W.; Hone, J. Measurement of the Elastic Properties and Intrinsic Strength of Monolayer Graphene. *Science* **2008**, *321*, 385–388.
46. Bauer, F.; Fousson, E.; Zhang, Q. M. Recent Advances in Highly Electrostrictive P(VDF-TrFE-CFE) Terpolymers. Dielectrics and Electrical Insulation. *IEEE Trans.* **2006**, *13*, 1149–1154.